Desired Compensation Adaptive Robust Control of a Linear-Motor-Driven Precision Industrial Gantry With Improved Cogging Force Compensation

Lu Lu, Zheng Chen, Bin Yao, *Member, IEEE*, and Qingfeng Wang

***Abstract*—This paper proposes a new model for cogging forces of linear motor systems. Sinusoidal functions of positions are used to effectively capture the largely periodic nature of cogging forces with respect to position, while B-spline functions are employed to account for the additional aperiodic part of cogging forces. This model is experimentally demonstrated to be able to capture both the periodic and nonperiodic characteristics of cogging force while having a linear parametrization form, which makes the online adaptive compensation of cogging forces possible and effective. A discontinuous-projection-based desired compensation adaptive robust controller (DCARC) is then constructed, which makes full use of the proposed cogging force model for an improved cogging force compensation. Comparative experimental results with various cogging force compensations are obtained on both axes of a linear-motor-driven industrial gantry. The results show that DCARC with the proposed model compensation achieves the best tracking performance among all the three algorithms tested, validating the proposed cogging force model. The excellent tracking performances obtained in the experiments also verify the effectiveness of the proposed ARC control algorithms in practical applications. The proposed model and control algorithm can be applied for other types of motor control systems as well.**

***Index Terms*—Adaptive control, cogging force, linear motors, motion control.**

I. Introduction

BEING one of the direct-drive devices [1]–[4], linear motors have received significant attention in recent researches [5]–[12] due to the hardware advantages of such a system for use in high-speed/high-accuracy positioning systems [13]. In controlling iron core linear motors with permanent magnets, cogging forces, which arise due to the strong attraction forces between the iron core and the permanent magnets, is a common phenomenon that cannot be ignored [8]. Thus, significant research efforts have been devoted to the modeling and compensation of cogging forces [8], [10], [14]–[18]. In [8], feedforward compensation terms based on an offline experimentally identified model of the first-order approximation of cogging forces are added to the position controller, which tends to be too sensitive and costly to be useful in practice. The cogging force in [10] and [14]–[16] is assumed to be a periodic function with respect to position. Fourier expansion is then utilized, with the choice of first few significant terms, to represent the cogging force. Based on this, compensation algorithms have been designed and implemented. In another type of research, such as [17] and [18], a neural-network-based learning feedforward controller is proposed to reduce the positional inaccuracy due to cogging forces or any other reproducible and slowly varying disturbances. But this method simply assumes the cogging force to be a general nonlinear function with respect to position, without considering its periodic nature. Furthermore, overall closed-loop stability is not guaranteed. In fact, it is observed in [17] that instability may occur at high-speed movements.

Cogging forces have periodic nature, but due to the complicated physical interactions among various magnets, they may show some aperiodic characteristics. In this paper, we conduct explicit measurement of cogging forces on both axes of a linear-motor-driven industrial gantry. The measured cogging forces exhibit certain periodic characteristics with respect to position, which corresponds well with the actual linear motor construction and can be represented by sinusoidal functions of positions with the unknown weights. However, the amplitude of the weights changes significantly with position, as can be observed from the measurement. Based on this observation, a new model is proposed, considering both the periodic and nonperiodic characteristics of cogging forces. Since the cogging force is largely periodic, we use sinusoidal functions of position to be part of basis functions. B-spline functions are then constructed to capture the changing amplitudes of sinusoidal functions with respect to position. The proposed model is experimentally demonstrated to be able to approximate cogging forces measured in the experiments well, by using a least-squares curve-fitting method.

As opposed to the traditional neural-network-based blind modeling of cogging forces [17], [18], the compactness and the linear-parametrization form of the proposed model make it a perfect choice for online adaptive cogging force compensation as well. To this end, a suitable model-based compensation algorithm should be designed. A good control algorithm should have features of strong disturbance rejection, performance robustness

Manuscript received March 22, 2008; revised June 27, 2008. Current version published December 17, 2008. Recommended by Technical Editor O. Kaynak. This work was supported in part by the U.S. National Science Foundation under Grant CMS-0600516 and in part by the National Natural Science Foundation of China (NSFC) under the Joint Research Fund for Overseas Chinese Young Scholars under Grant 50528505.

L. Lu was with the State Key Laboratory of Fluid Power Transmission and Control, Zhejiang University, Hangzhou 310027, China. He is now with the School of Mechanical Engineering, Purdue University, West Lafayette, IN 47907 USA (e-mail: lulu.lvlv@gmail.com).

Z. Chen and Q. Wang are with the State Key Laboratory of Fluid Power Transmission and Control, Zhejiang University, Hangzhou 310027, China (e-mail: cwlinus@gmail.com).

B. Yao is with the School of Mechanical Engineering, Purdue University, West Lafayette, IN 47907 USA, and also with the Mechatronic Systems Innovation Platform, State Key Laboratory of Fluid Power Transmission and Control, Zhejiang University, Hangzhou 310027, China (e-mail: byao@purdue.edu).

Color versions of one or more of the figures in this paper are available online at http://ieeexplore.ieee.org

Digital Object Identifier 10.1109/TMECH.2008.2003510

to model uncertainties, and the ability of online learning (e.g., parameter adaptation) in reducing model uncertainties to maximize the achievable control performance. The idea of adaptive robust control (ARC) [19]–[21] incorporates the merits of deterministic robust control (DRC) and adaptive control (AC), which guarantees certain robust performance in the presence of uncertainties while having a controlled robust learning process for better control performance. The ARC has been extended to the desired compensation ARC (DCARC) in [22] and [23], and for repetitive tasks in [24] where explicit modeling of cogging forces is not needed except the period of the repetitive tasks.

In the second half of this paper, a DCARC algorithm is designed, making full use of the proposed cogging force model. Unlike in [24], the tasks to be performed need not be periodic, and the obtained results are more general and have much wider applications. The algorithm is then tested on a two-axis iron core linear-motor-driven industrial gantry with significant cogging force effect. Comparative experimental results with each axis running separately show an improved performance over the previously obtained results with DCARCs [25] for both axes after using the proposed cogging force model, though the two axes have different measured cogging force patterns that are assumed to be unknown to users in the controller designs. These results validate the usefulness of the proposed cogging force model for linear motor controls and the excellent tracking performance of the proposed DCARC in practical applications.

II. Modeling and Problem Formulation

The dynamics of 1-DOF linear motor systems can be represented by the following equation [26], [27]:

$$M\ddot{x} + B\dot{x} + F_c(\dot{x}) + F_r(x) = u + d \tag{1}$$

where x represents the position of a linear motor, with its velocity and acceleration denoted as $\dot{x}$ and $\ddot{x}$, respectively. M and B are the mass and viscous friction coefficient, respectively. $F_c(\dot{x})$ represents the Coulomb friction term that is modeled by

$$F_c(\dot{x}) = A_f S_f(\dot{x}) \tag{2}$$

where A_f represents the unknown Coulomb friction coefficient and $S_f(\dot{x})$ is a known continuous or smooth function used to approximate the traditional discontinuous sign function $\mathrm{sgn}(\dot{x})$ used in the traditional Coulomb friction modeling for effective friction compensation in implementation [14]. In (1), $F_r(x)$ represents the position-dependent cogging force, u the control input force, and d the lumped effect of external disturbances and various types of modeling errors.

Traditionally, cogging forces are assumed to be periodic functions with respect to position [26]. As a result, it can be represented by $F_r(x) = \sum_{i=1}^{\infty}(S_i \sin[(2i\pi/P)x] + C_i \cos[(2i\pi/P)x])$, where P is the pitch of the magnet pairs, and S_i and C_i are some constants. Practically, we can select the first few important terms and ignore all higher terms, i.e., i varies from 0 to a positive integer n. This equation can well explain the periodic phenomena of cogging force and has been widely used in compensation algorithms [14]–[16], [25].

However, due to many complicated physical effects, such as the differences among magnets, the actual cogging force may not be exactly periodic. In the experimental section of this paper, we measure the cogging forces explicitly using a force sensor. It can be observed that the amplitudes of sinusoidal functions vary with the change of position. Thus, using the periodic assumption may lead to a rather inaccurate modeling of cogging force. In order to capture the actual cogging force more precisely to achieve better tracking control performances, it is necessary to assume S_i and C_i to be functions of position, namely $S_i = f_{Si}(x)$ and $C_i = f_{Ci}(x)$. With such a varying amplitude modification to periodic functions, the cogging force model becomes

$$F_r(x) = \sum_{i=1}^{n}\left[f_{Si}(x)\sin\left(\frac{2i\pi}{P}x\right) + f_{Ci}(x)\cos\left(\frac{2i\pi}{P}x\right)\right]. \tag{3}$$

The selection of f_{Sin} and f_{Cin} should also make full use of the available physical characteristics of cogging forces to ease the design of effective online adaptive cogging force compensation. To this end, B-spline functions [28] are utilized to give a mathematical model of f_{Si} and f_{Ci}, respectively. Namely, f_{Si} and f_{Ci} are chosen as

$$f_{Si}(x) = \sum_{j=1}^{m} N_{j,k}(x) S_{ij}$$
$$f_{Ci}(x) = \sum_{j=1}^{m} N_{j,k}(x) C_{ij} \tag{4}$$

where definitions are given in (5), as shown at the bottom of the page, where k is the order of the B-spline and m is the number of control points needed. $[X_1, X_2, \ldots, X_{m+k-1}, X_{m+k}]$ is the knot vector, with $X_{j+1} \geq X_j$ defined to be as follows. Let m be the number of magnet segments on the linear motor axis. If a kth-order B-spline function is used, then X_k is defined to be the position of the first magnet and X_{k+m} the position of the last magnet, with X_{k+j} as the position of the $(j+1)$th magnet. By the construction of a linear motor, $X_{k+j} = X_k + jP,\ j = 1, \ldots, m$. So, define $X_1, \ldots, X_{k-1}$ as $X_{k-j} = X_k - jP,\ j = 1, \ldots, k-1$. Using a B-spline function has the following merits.

1) The increment of neighboring elements in the knot vector of a B-spline function is selected as the physical pitch of magnets on the linear motor axis, i.e., $X_{j+1} - X_j = P$. This means that the value of the B-spline function changes with the unit of magnets' pitch. Physically, it can interpret

$$\begin{cases} N_{j,k}(x) = \begin{cases} 1, & \text{when } x \in [X_j,\ X_{j+1}) \\ 0, & \text{else} \end{cases}, & k = 1 \\ N_{j,k}(x) = \dfrac{x - X_j}{X_{j+k-1} - X_j} N_{j,k-1}(x) + \dfrac{X_{j+k} - x}{X_{j+k} - X_{j+1}} N_{j+1,k-1}(x), & k \geq 2 \end{cases} \tag{5}$$

the changing amplitude of a sinusoidal function caused by the difference of each magnet.

2) The B-spline function is linear to the control points (S_{ij} and C_{ij}). The resulting cogging force model described by (3) and (4) is thus linearly parametrized by the control points (S_{ij} and C_{ij}) with known basis functions. Such a model significantly simplifies the online estimate of unknown control points for adaptive compensation of cogging forces.
3) The basis function $N_{j,k}(x)$ is active only when $x \in [X_j, X_{j+k})$. It is zero in all other regions. Such a nice property is especially preferable for real-time adaptive controls and automated online modeling [29], because in every sampling period, we only have to fetch a small portion of online parameter estimates from memory for compensation and update once we decide where the current position is. For example, when $x \in [X_l, X_{l+1})$ for some l, only $S_{i(l-k+1)},\ C_{i(l-k+1)}, \ldots, S_{il},\ C_{il}$ are needed for update and compensation. All other coefficients have zero values for corresponding basis functions and need not be considered. Thus, the algorithm is economic, especially when k is chosen to be small.

Combining (3) and (4), the cogging force $F_r(x)$ is put in a concise form as

$$F_r(x) = A_r^T S_r(x) \tag{6}$$

where $A_r = [S_{11},\ C_{11}, \ldots,\ S_{ji},\ C_{ji}, \ldots,\ S_{mn},\ C_{mn}]^T \in R^{2mn}$ is the vector of unknown control points and

$$S_r = \left[N_{1,k}(x)\sin\left(\frac{2\pi}{P}x\right),\ N_{1,k}(x)\cos\left(\frac{2\pi}{P}x\right), \ldots, N_{j,k}(x)\sin\left(\frac{2i\pi}{P}x\right),\ N_{j,k}(x)\cos\left(\frac{2i\pi}{P}x\right), \ldots, N_{m,k}(x)\sin\left(\frac{2n\pi}{P}x\right),\ N_{m,k}(x)\cos\left(\frac{2n\pi}{P}x\right)\right]^T \tag{7}$$

is the vector of known basis functions. With this cogging force model, the linear motor dynamics (1) can be linearly parameterized as

$$M\ddot{x} + B\dot{x} + A_f S_f(\dot{x}) + A_r^T S_r(x) - d_n = u + \tilde{d} \tag{8}$$

where d_n denotes the nominal value of d and $\tilde{d} = d - d_n$ represents the time-varying portion of the lumped uncertainties. Equation (8) can also be put in a state-space form of

$$\dot{x}_1 = x_2 \tag{9}$$

$$M\dot{x}_2 = u - Bx_2 - A_f S_f(x_2) - A_r^T S_r(x_1) + d_n + \tilde{d} \tag{10}$$

where x_1 and x_2 are the position and velocity, respectively.

Let $x_d(t)$ be the desired motion trajectory, which is assumed to be known, bounded with bounded derivatives up to the second order. The objective is to synthesize a bounded control input u such that the output x_1 tracks $x_d(t)$ as closely as possible in spite of various modeling uncertainties.

III. Adaptive Robust Control (ARC)

A. Assumptions

The left-hand side of (8) is the sum of known functions times unknown parameters. Let us denote the unknown parameter set as $\theta = [M,\ B,\ A_f,\ A_r^T,\ -d_n]^T \in R^{4+2mn}$, with $\theta_1 = M$, $\theta_2 = B$, $\theta_3 = A_f$, $\theta_{4b} = A_r$, $\theta_5 = -d_n$. In order to design a bounded control law with guaranteed transient performance, the following practical assumption is made.

Assumption 1: The extent of the parametric uncertainties and uncertain nonlinearities are known, i.e.,

$$\theta \in \Omega_\theta \triangleq \{\ \theta :\ \ \theta_{\min} < \theta < \theta_{\max}\ \} \tag{11}$$

$$\tilde{d} \in \Omega_d \triangleq \{\ \tilde{d} :\ \ |\tilde{d}| \le \delta_d\ \} \tag{12}$$

where $\theta_{\min} = [\theta_{1\min}, \ldots, \theta_{(4+2mn)\min}]^T$, $\theta_{\max} = [\theta_{1\max}, \ldots, \theta_{(4+2mn)\max}]^T$, and δ_d are known. ♢

B. Notations and Discontinuous Projection

Let $\hat{\theta}$ denote the estimate of θ and $\tilde{\theta}$ the estimation error (i.e., $\tilde{\theta} = \hat{\theta} - \theta$). In view of (11), the following discontinuous-projection-type adaptation law will be used:

$$\dot{\hat{\theta}} = \mathrm{Proj}_{\hat{\theta}}(\Gamma\tau) \tag{13}$$

where $\Gamma > 0$ is a diagonal matrix and τ is an adaptation function to be synthesized later. The projection mapping $\mathrm{Proj}_{\hat{\theta}}(\bullet) = [\mathrm{Proj}_{\hat{\theta}_1}(\bullet_1), \ldots, \mathrm{Proj}_{\hat{\theta}_5}(\bullet_5)]^T$ is defined in element as

$$\mathrm{Proj}_{\hat{\theta}_i}(\bullet_i) = \begin{cases} 0, & \text{if } \hat{\theta}_i = \theta_{i\max} \text{ and } \bullet_i > 0 \\ 0, & \text{if } \hat{\theta}_i = \theta_{i\min} \text{ and } \bullet_i < 0 \\ \bullet_i, & \text{otherwise.} \end{cases} \tag{14}$$

C. Adaptive Robust Control Law Synthesis

Define a switching-function-like quantity p as

$$p \triangleq \dot{e} + k_1 e = x_2 - x_{2eq}, \qquad x_{2eq} \triangleq \dot{x}_d - k_1 e \tag{15}$$

where $e = x_1 - x_d(t)$ is the output tracking error and $k_1 > 0$ is a positive gain. If p is small or converges to zero, then the output tracking error e will be small or converge to zero since $G_p(s) = e(s)/p(s) = 1/(s + k_1)$ is a stable transfer function. So, the rest of the design is to make p as small as possible. Differentiating (15) and noting (10), one obtains

$$\begin{aligned} M\dot{p} &= u - \theta_1\dot{x}_{2eq} - \theta_2 x_2 - \theta_3 S_f - \theta_{4b}^T S_r - \theta_5 + \tilde{d} \\ &= u + \varphi^T\theta + \tilde{d} \end{aligned} \tag{16}$$

where $\dot{x}_{2eq} \triangleq \ddot{x}_d - k_1\dot{e}$ and $\varphi^T = [-\dot{x}_{2eq},\ -x_2, -S_f(x_2),\ -S_r(x_1),\ -1]$. We propose the following ARC control law:

$$u = u_a + u_s, \qquad u_a = -\varphi^T\hat{\theta} \tag{17}$$

where u_a is the adjustable model compensation needed for perfect tracking and u_s is the robust control law to be synthesized later. Substituting (17) into (16), and then simplifying the resulting expression, one obtains

$$M\dot{p} = u_s - \varphi^T\tilde{\theta} + \tilde{d}. \tag{18}$$

The robust control function u_s has the following structure:

$$u_s = u_{s1} + u_{s2}, \qquad u_{s1} = -k_2 p \tag{19}$$

where u_{s1} is a simple proportional feedback to stabilize the nominal system and u_{s2} is a robust performance feedback term having the following properties [21], [20]:

$$p\{u_{s2} - \varphi^T \tilde{\theta} + \tilde{d}\} \le \varepsilon$$
$$p u_{s2} \le 0 \tag{20}$$

where ε is a design parameter that can be arbitrarily small. With the proposed control law, we have the following theorem that can be proved using the same technique as in [26].

Theorem 1: If the adaptation function in (13) is chosen as

$$\tau = \varphi p \tag{21}$$

then the ARC control law (17) guarantees the following.

A) In general, all signals are bounded. Furthermore, the positive-definite function V_s defined by

$$V_s = \frac{1}{2} M p^2 \tag{22}$$

is bounded above by

$$V_s(t) \le \exp(-\lambda t) V_s(0) + \frac{\varepsilon}{\lambda}[1 - \exp(-\lambda t)] \tag{23}$$

where $\lambda = 2k_2/\theta_{1\max}$.

B) If after a finite time t_0, there exist parametric uncertainties only (i.e., $\tilde{d} = 0 \quad \forall t \ge t_0$), then, in addition to results in A), zero final tracking error is also achieved, i.e., $e \longrightarrow 0$ and $p \longrightarrow 0$ as $t \longrightarrow \infty$.

D. Desired Compensation Adaptive Robust Control

DCARC uses desired trajectory signals to form regressor, which has been shown to outperform ARC in terms of all indexes [27]. Following the same design procedure as in [25], a DCARC law using the proposed cogging force model is also constructed as follows.

By applying the mean value theorem, we have

$$S_f(x_2) - S_f(\dot{x_d}) = g_f(x_2, t)\dot{e} \tag{24}$$
$$S_r(x_1) - S_r(x_d) = g_r(x_1, t) e \tag{25}$$

where $g_f(x_2, t)$ and $g_r(x_1, t)$ are certain nonlinear functions. The control law is thus given by

$$u = u_a + u_s, \qquad u_a = -\varphi_d^T \hat{\theta} \tag{26}$$
$$u_s = u_{s1} + u_{s2}, \qquad u_{s1} = -k_{s1} p \tag{27}$$
$$\dot{\hat{\theta}} = \mathrm{Proj}_{\hat{\theta}}(\Gamma \varphi_d p) \tag{28}$$

where $\varphi_d^T = [-\ddot{x}_d,\ -\dot{x}_{1d},\ -S_f(\dot{x}_d),\ -S_r(x_d),\ -1]$ is the regressor using the desired trajectory signals. k_{s1} is a nonlinear gain large enough such that the following matrix is positive definite:

$$\begin{bmatrix} -k_2 + k_{s1} - \theta_1 k_1 + \theta_2 + \theta_3 g_f & -\frac{1}{2}\left(k_1\theta_2 + k_1\theta_3 g_f - \theta_{4b}^T g_r\right) \\ -\frac{1}{2}\left(k_1\theta_2 + k_1\theta_3 g_f - \theta_{4b}^T g_r\right) & \frac{1}{2} M k_1^3 \end{bmatrix}. \tag{29}$$

Fig. 1. Gantry-type industrial linear motor drive system.

Further, u_{s2} is a robust feedback term satisfying

$$p\{u_{s2} - \varphi_d^T \tilde{\theta} + \tilde{d}\} \le \varepsilon$$
$$p u_{s2} \le 0 \tag{30}$$

where ε is a design parameter that can be arbitrarily small. It can be proved using the same technique as in [27] that the following theorem holds.

Theorem 2: The DCARC control law (26) guarantees the following.

A) In general, all signals are bounded. Furthermore, the positive-definite function V_s defined by

$$V_s = \frac{1}{2} M p^2 + \frac{1}{2} M k_1^2 e^2 \tag{31}$$

is bounded above by

$$V_s(t) \le \exp(-\lambda t) V_s(0) + \frac{\varepsilon}{\lambda}[1 - \exp(-\lambda t)] \tag{32}$$

where $\lambda = \min\{2k_2/\theta_{1\max},\ k_1\}$.

B) If after a finite time t_0, there exist parametric uncertainties only (i.e., $\tilde{d} = 0 \quad \forall t \ge t_0$), then, in addition to results in A), zero final tracking error is also achieved, i.e., $e \longrightarrow 0$ and $p \longrightarrow 0$ as $t \longrightarrow \infty$.

IV. Experimental Results

A. Experimental Setup

In the Precision Mechatronics Laboratory at Zhejiang University, a two-axis commercial Anorad HERC-510-510-AA1-B-CC2 Gantry by Rockwell Automation has been set up, as shown in Fig. 1. Both axes of the gantry are powered by Anorad LC-50-200 iron core linear motors and have a travel distance of 0.51 m. Linear encoders provide both axes a position measurement resolution of 0.5 μm. The entire system will be used as motion system hardware for our study. To implement real-time control algorithm, the previous system is connected to a dSPACE CLP1103 controller board.

B. System Identification

Experiments have been conducted on the X-axis and Y-axis separately. First, offline parameter identification is carried out, and it is found that nominal values of the system parameters without loads are $M = 0.12\ \mathrm{V/m \cdot s^2}$, $B = 0.166\ \mathrm{V/m \cdot s}$,

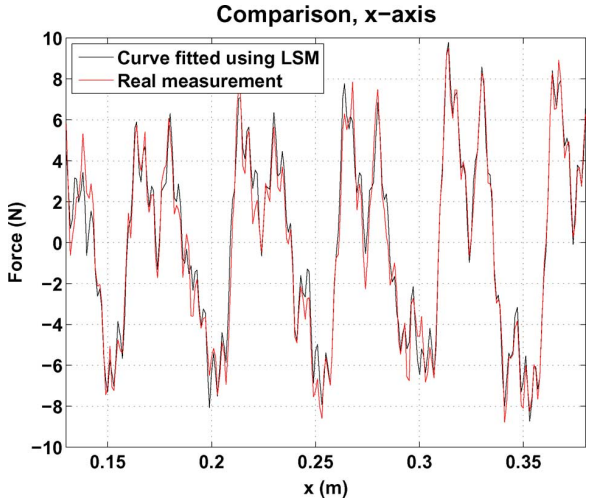

Fig. 2. Measured cogging forces of X-axis and its curve fitting.

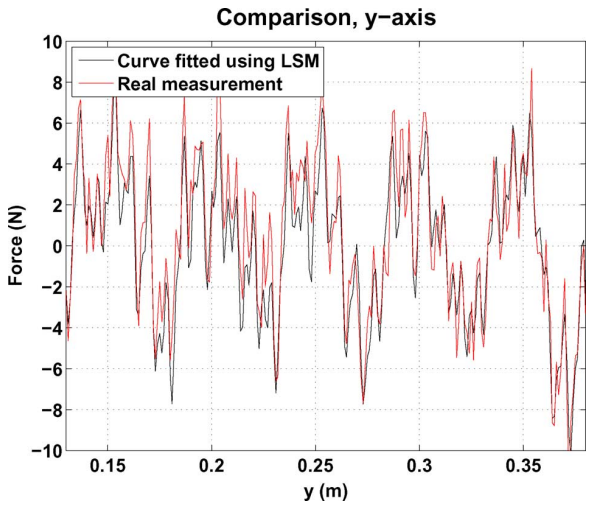

Fig. 3. Measured cogging forces of Y-axis and its curve fitting.

$A_f = 0.15$ V for X-axis, and $M = 0.64\ \mathrm{V/m \cdot s^2}, B = 0.24\ \mathrm{V/m \cdot s}$, $A_f = 0.606$ V for Y-axis, where all values shown are normalized with respect to the input voltage in terms of $volts$ sent to the linear motors. In addition, the gain from the input voltage to the force applied to the mechanical system is computed as $k_f = 69$ N/V, through the measurement of input voltage to the system and the resultant force when the motor is blocked.

Explicit measurement of cogging force is then conducted for both axes by blocking the motor and using an external force sensor (HBM U10M Force Transducer with AE101 Amplifier) to measure the blocking forces at zero input voltages. This measurement is done for various positions with 1-mm incremental distance. The measured cogging forces are shown in Fig. 2 for X-axis and Fig. 3 for Y-axis, respectively. As can be seen from the figures, cogging forces of both axes have periodic characteristics with respect to position, with the fundamental period corresponding to the pitch of the magnets ($P = 50$ mm). However, it is also observed that the amplitude of this largely periodic function vary significantly in the travel range. To accurately capture the cogging force, we need more than sinusoidal functions of positions.

The method proposed in this paper is then used to approximate the measured cogging forces. After applying fast Fourier transform (FFT) to Figs. 2 and 3, it is observed that the harmonic terms of cogging forces for both axes have significant values at frequencies corresponding to $i = 1,\ 2,\ 3,\ 6$, and 12 in (3). So these five frequencies are kept when approximating cogging forces. Third-order B-spline functions are used to capture the change of amplitudes of cogging forces during the travel range. A curve fitting using the standard least square method (LSM) is then performed to obtain the values of B-spline control points in (6) that best approximate the measured cogging forces. The output of the resulting cogging force models are plotted against the measured ones in Fig. 2 for X-axis and in Fig. 3 for Y-axis. As can be seen from the figures, though slight differences exist due to the finite number of frequencies used in approximation, the proposed cogging force model well captures the largely periodic nature as well as the changing amplitude of cogging force with respect to position.

C. Comparative Experimental Results for X-Axis

For X-axis, the dSPACE controller's sampling frequency is selected as $f_s = 5$ kHz, which results in a velocity measurement resolution of 0.0025 m/s for the linear encoder feedback. The following three control algorithms are compared:

- *C1* DCARC without cogging force compensation;
- *C2* DCARC with cogging force compensation based on periodic cogging force models [14], [25];
- *C3* DCARC with cogging force compensation based on the proposed model.

To have a fair comparison, all the controller parameters of these three algorithms are chosen to be the same when they have the same meaning. Namely, the lower and upper bounds of the parameter variations for M, B, A_f, and d for X-axis are chosen as $[0.1,\ 0.15,\ 0.1,\ -0.5]$ and $[0.2,\ 0.35,\ 0.3,\ 0.5]$, respectively. The upper and lower bounds of all coefficients of A_r in both the algorithms $C2$ and $C3$ are set as 0.1 and -0.1, respectively. For all control algorithms, the feedback gains are set at $k_1 = 200$ and $k_{s1} = 400 \times 0.12$, with the adaptation gains for M, B, A_f, and d chosen as $[1,\ 10,\ 10,\ 1000]$. The adaptation gains for all coefficients in A_r are chosen as 100. For algorithm $C3$, third-order B-spline along with the first three harmonic frequencies ($i = 1, 2, 3$) are used for the online cogging force compensation model.

As in [14] and [25], the desired trajectory used represents point-to-point movements, typical in manufacture industry, with a travel distance of 0.4 m, a maximum velocity of 0.5 m/s, and a maximum acceleration of 10 m/s^2. Fig. 4 shows the tracking error of three algorithms after running the linear motor for a while, with the magnified plot over a single running period shown in Fig. 5. From these error plots, it is observed that the steady-state position tracking errors of all the algorithms are within the linear encoder resolution of 0.5 μm when the system comes to a stop and within 20 μm during the acceleration and deceleration

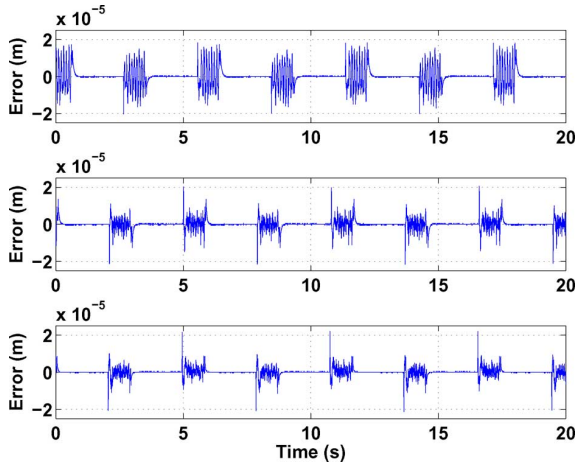

Fig. 4. Tracking errors of three DCARCs, X-axis.

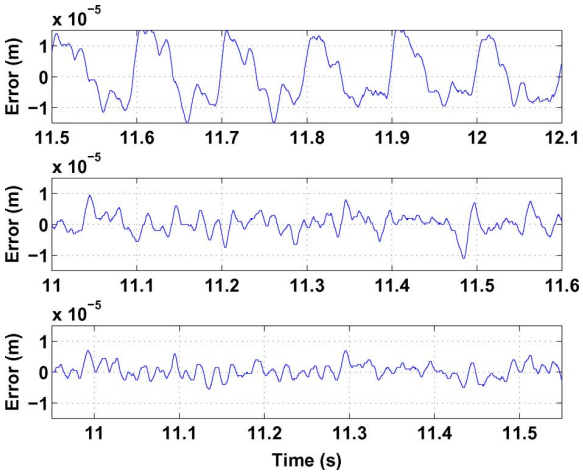

Fig. 5. Magnification of tracking errors over one running period, X-axis.

TABLE I
PERFORMANCE INDEX, X-AXIS

Algorithms	$\|e\|_\infty$ (m)	$\|e\|_2$ (m)
C1	1.6500e-005	8.3408e-006
C2	1.1000e-005	3.1064e-006
C3	6.9996e-006	2.3043e-006

periods, demonstrating the excellent tracking performances of the proposed DCARC algorithms. It is also seen that the tracking errors are quite different during the constant-speed motion period. Namely, with the periodic cogging force compensation, the tracking error is substantially reduced in DCARC $C2$ when compared to DCARC $C1$ with no cogging force compensation. The tracking error is further reduced with the proposed cogging force compensation, with the cogging force shape of tracking error plot no longer evident, revealing a smoother constant-speed movement. Table I shows the performance indexes for the three algorithms. It is also evident from these quantitative measures that the proposed algorithm outperforms the other two. In addition, for algorithms $C2$ and $C3$, a part of the input control force $k_f \hat{\theta}_{4b}^T S_r(x_d)$, which represents the online estimation of cogging forces, is plotted for the constant-speed motion period,

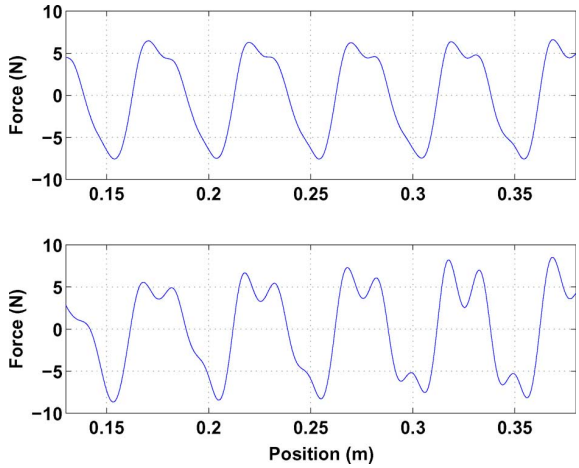

Fig. 6. Online estimation of cogging forces (upper figure for algorithm $C2$ and lower figure for algorithm $C3$), X-axis.

as in Fig. 6. As can be observed from these plots, the online estimation of cogging forces by algorithm $C3$ quite faithfully capture the changing amplitude of sinusoidal functions with respect to position, as compared to the explicit measurement of cogging forces in Fig. 2, while the online estimation of cogging forces by algorithm $C2$ is almost a periodic function of position, failing to represent the aperiodic characteristics of the real cogging forces.

D. Comparative Experimental Results for Y-Axis

The aforementioned three DCARC algorithms are also tested and compared on Y-axis of the Anorad gantry, which has a quite different measured cogging force pattern than that of X-axis. The dSPACE controller's sampling frequency is also selected as $f_s = 5$ kHz. In all the three algorithms, the lower and upper bounds of the parameter variations for M, B, A_f, and d are chosen as $[0.5,\ 0.1,\ 0.3,\ -0.8]$ and $[0.75,\ 0.3,\ 0.8,\ 0.8]$, respectively. As to A_r, we select all the upper bounds of its coefficients as 0.2 and lower bounds as -0.2, for both algorithms $C2$ and $C3$. $k_1 = 100$ and $k_{s1} = 150 \times 0.64$ for all algorithms. The adaptation gains for M, B, A_f, and d are chosen as $[1,\ 10,\ 10,\ 1000]$. The adaptation gains for all coefficients in A_r are chosen as 100. For algorithm $C3$, third-order B-spline with three harmonic frequencies ($i = 1, 6, 12$) are used for online cogging force compensation. A desired trajectory with 0.1 m/s as the maximum velocity and 1 m/s^2 as the maximum acceleration is used in all experiments.

Fig. 7 shows the tracking errors of three algorithms after running the linear motor for a while with the magnified plot of errors over a single running period shown in Fig. 8. As seen from these figures, during the constant-speed periods, the tracking error is reduced a little bit when using the periodic cogging force compensation (algorithm $C2$). But the shape of cogging force is still evident in the tracking error plot. However, such a shape cannot be observed in the tracking error plot with the proposed cogging force compensation anymore, indicating a smoother constant-speed motion. Table II shows the performance indexes for the three algorithms. Again, a significantly improved control

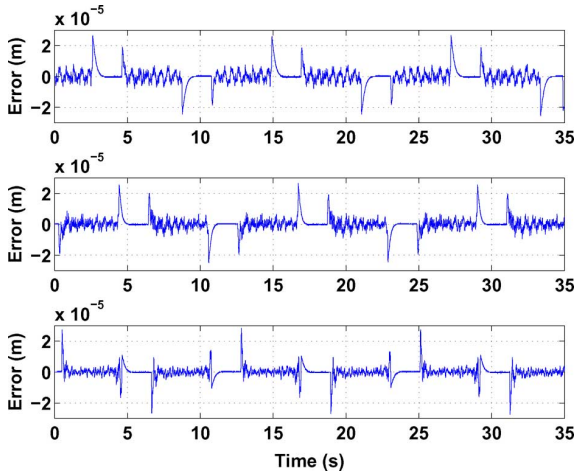

Fig. 7. Tracking errors of three DCARCs, Y-axis.

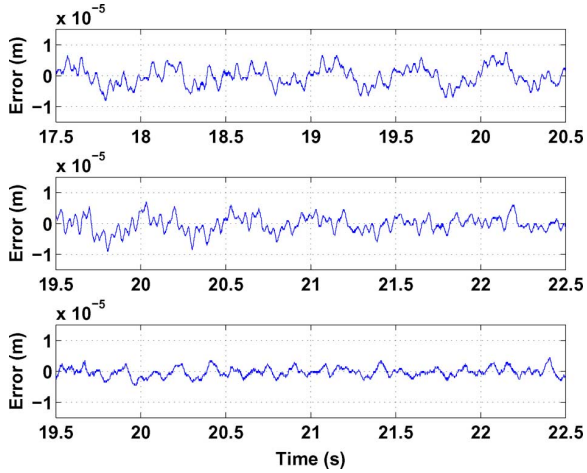

Fig. 8. Magnification of tracking errors over one running period, Y-axis.

TABLE II
PERFORMANCE INDEX, Y-AXIS

Algorithms	$\|e\|_\infty$ (m)	$\|e\|_2$ (m)
C1	8.0002e-006	3.0642e-006
C2	9.0003e-006	2.5790e-006
C3	4.5002e-006	1.5096e-006

performance is seen for the proposed algorithm $C3$, except during the very short high-acceleration/deceleration periods where the maximum tracking errors of the three algorithms are comparable as modeling uncertainties in those periods are dominated by factors other than cogging force compensations (e.g., inertia, friction, and sampling effects). All these results demonstrate the effectiveness of the proposed cogging force compensation in practical applications. Same as in the X-axis experiments, a part of the input control force $k_f \hat{\theta}_{4b}^T S_r(x_d)$ is plotted in Fig. 9 for the constant-speed motion period, and for algorithms $C2$ and $C3$, respectively. As can be observed from these plots, the online estimation of cogging forces by algorithm $C2$ has a larger amplitude than the actual one. By comparison, the online estimation of cogging forces by the proposed algorithm $C3$ is able to largely capture the trend of changing amplitude of the measured

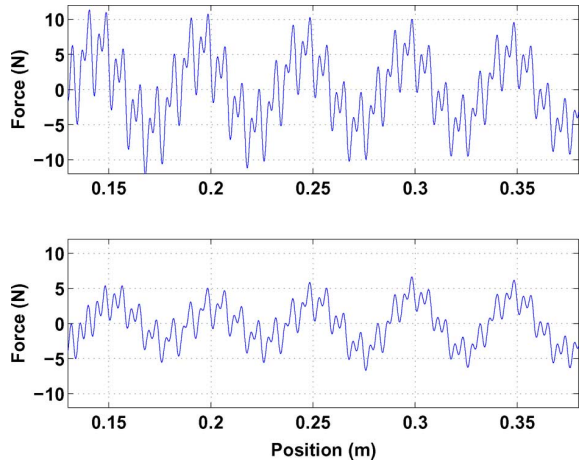

Fig. 9. Online estimation of cogging forces (upper figure for algorithm $C2$ and lower figure for algorithm $C3$), Y-axis.

cogging forces, leading to an improved tracking performance, as shown in Fig. 8.

V. CONCLUSION

In this paper, a new cogging force model capable of capturing both the periodic and nonperiodic characteristics of cogging forces has been proposed. The linearly parametrized form and the computational efficiency of the localized B-spline functions also lend the proposed model an ideal choice for online adaptive cogging force compensation. Adaptive robust control algorithms making full use of the proposed cogging force model are also developed for linear motor controls. The proposed algorithms have been implemented on a linear-motor-driven two-axis commercial industrial gantry system. Comparative experimental results show that smaller tracking error and smoother constant-speed motion are obtained using the ARC algorithm with the proposed cogging force compensation than with periodic cogging force compensation only, demonstrating the effectiveness of the proposed algorithms in practical applications. It is noted that the proposed model and control algorithm can be used for other types of motor control systems as well.

REFERENCES

[1] H. Son and K. M. Lee, "Distributed multipole models for design and control of PM actuators and sensors," *IEEE/ASME Trans. Mechatronics*, vol. 13, no. 2, pp. 228–238, Apr. 2008.

[2] L. Yan, I. Chen, C. Lim, G. Yang, W. Lin, and K. M. Lee, "Design and analysis of a permanent magnet spherical actuator," *IEEE/ASME Trans. Mechatronics*, vol. 13, no. 2, pp. 239–248, Apr. 2008.

[3] T. Hu and W. J. Kim, "Extended range six-DOF high-precision positioner for wafer processing," *IEEE/ASME Trans. Mechatronics*, vol. 11, no. 6, pp. 682–689, Dec. 2006.

[4] B. Bona, M. Indri, and N. Smaldone, "Rapid prototyping of a model-based control with friction compensation for a direct-drive robot," *IEEE/ASME Trans. Mechatronics*, vol. 11, no. 5, pp. 576–584, Oct. 2006.

[5] D. M. Alter and T. C. Tsao, "Control of linear motors for machine tool feed drives: Design and implementation of H_∞ optimal feedback control," *Trans. ASME, J. Dyn. Syst., Meas., Control*, vol. 118, pp. 649–656, 1996.

[6] S. Komada, M. Ishida, K. Ohnishi, and T. Hori, "Disturbance observer-based motion control of direct drive motors," *IEEE Trans. Energy Convers.*, vol. 6, no. 3, pp. 553–559, Sep. 1991.

[7] T. Egami and T. Tsuchiya, "Disturbance suppression control with preview action of linear dc brushless motor," *IEEE Trans. Ind. Electron.*, vol. 42, no. 5, pp. 494–500, Oct. 1995.
[8] P. V. Braembussche, J. Swevers, H. V. Brussel, and P. Vanherck, "Accurate tracking control of linear synchronous motor machine tool axes," *Mechatronics*, vol. 6, no. 5, pp. 507–521, 1996.
[9] H. Fujimoto and B. Yao, "Multirate adaptive robust control for discrete-time non-minimum phase systems and application to linear motors," *IEEE/ASME Trans. Mechantronics*, vol. 10, no. 4, pp. 371–377, Aug. 2005.
[10] S. Zhao and K. Tan, "Adaptive feedforward compensation of force ripples in linear motors," *Control Eng. Pract.*, vol. 13, pp. 1081–1092, 2005.
[11] Y. Hong and B. Yao, "A globally stable high performance adaptive robust control algorithm with input saturation for precision motion control of linear motor drive system," *IEEE/ASME Trans. Mechatronics*, vol. 12, no. 2, pp. 198–207, Apr. 2007, (Part of the paper appeared in *Proc. IEEE/ASME Conf. Adv. Intell. Mechatronics (AIM 2005)*, pp. 1623–1628).
[12] C.-I. Huang and L.-C. Fu, "Adaptive approach to motion controller of linear induction motor with friction compensation," *IEEE/ASME Trans. Mechatronics*, vol. 12, no. 4, pp. 480–490, Aug. 2007.
[13] F. Aghili, J. M. Hollerbach, and M. Buehler, "A modular and high-precision motion control system with an integrated motor," *IEEE/ASME Trans. Mechatronics*, vol. 12, no. 3, pp. 317–328, Jun. 2007.
[14] L. Xu and B. Yao, "Adaptive robust precision motion control of linear motors with ripple force compensation: Theory and experiments," in *Proc. IEEE Conf. Control Appl.*, Anchorage, AK, 2000, pp. 373–378 (Winner of the Best Student Paper Competition).
[15] C. Roehrig, "Force ripple compensation of linear synchronous motors," *Asian J. Control*, vol. 7, pp. 1–11, Mar. 2005.
[16] T.-S. Hwang, J.-K. Seok, and D.-H. Kim, "Active damping control of linear hybrid stepping motor for cogging force compensation," *IEEE Trans. Magn.*, vol. 42, no. 2, pp. 329–334, Feb. 2006.
[17] G. Otten, T. Vries, J. Amerongen, A. Rankers, and E. Gaal, "Linear motor motion control using a learning feedforward controller," *IEEE/ASME Trans. Mechatronics*, vol. 2, no. 3, pp. 179–187, Sep. 1997.
[18] Z. Lin, D. S. Reay, B. W. Williams, and X. He, "Torque ripple reduction in switched reluctance motor drives using B-spline neural networks," *IEEE Trans. Ind. Appl.*, vol. 42, no. 6, pp. 1445–1453, Nov./Dec. 2006.
[19] B. Yao and M. Tomizuka, "Smooth robust adaptive sliding mode control of robot manipulators with guaranteed transient performance," *Trans. ASME, J. Dyn. Syst., Meas. Control*, vol. 118, no. 4, pp. 764–775, 1996.
[20] B. Yao and M. Tomizuka, "Adaptive robust control of SISO nonlinear systems in a semi-strict feedback form," *Automatica*, vol. 33, no. 5, pp. 893–900, 1997 (Part of the paper appeared in *Proc. 1995 Amer. Control Conf.*, pp. 2500–2505, Seattle, WA).
[21] B. Yao, "High performance adaptive robust control of nonlinear systems: A general framework and new schemes," in *Proc. IEEE Conf. Decis. Control*, San Diego, CA, 1997, pp. 2489–2494.
[22] B. Yao, "Desired compensation adaptive robust control," in *Proc. ASME Dyn. Syst. Control Division, IMECE*, Anaheim, CA, DSC-Vol. 64, 1998, pp. 569–575 (The revision will appear in *Trans. ASME, J. Dyn. Syst. Meas. Control)*.
[23] Y. Hong and B. Yao, "A globally stable saturated desired compensation adaptive robust control for linear motor systems with comparative experiments," *Automatica*, vol. 43, no. 10, pp. 1840–1848, 2007 (Part of the paper appeared in *Proc. Amer. Control Conf.*, 2006, pp. 4760–4765).
[24] B. Yao and L. Xu, "On the design of adaptive robust repetitive controllers," in *Proc. ASME Int. Mech. Eng. Congr. Expo. (IMECE), DSC-3B-4*, 2001, pp. 1–9.
[25] B. Yao, C. Hu, and Q. Wang, "Adaptive robust precision motion control of high-speed linear motors with on-line cogging force compensations," in *Proc. IEEE/ASME Conf. Adv. Intell. Mechatronics*, Zurich, Switzerland, Sep. 2007, pp. 1–6.
[26] B. Yao and L. Xu, "Adaptive robust control of linear motors for precision manufacturing," *Int. J. Mechatronics*, vol. 12, no. 4, pp. 595–616, 2002 (Part of the paper appeared in *Proc. 14th IFAC World Congress*, Beijing, China, 1999, vol. A, pp. 25–30).
[27] L. Xu and B. Yao, "Adaptive robust precision motion control of linear motors with negligible electrical dynamics: Theory and experiments," *IEEE/ASME Trans. Mechatronics*, vol. 6, no. 4, pp. 444–452, Dec. 2001.
[28] C. de Boor, *A Practical Guide to Splines*. New York: Springer-Verlag, Dec. 2001.
[29] S. Liu and B. Yao, "Automated modeling of cartridge valve flow mapping," *IEEE/ASME Trans. Mechatronics*, vol. 11, no. 4, pp. 381–388, Aug. 2006.

Lu Lu received the B.Eng degree in mechatronic engineering from Zhejiang University, Hangzhou, China, in 2008. He is currently working toward the Ph.D. degree in the School of Mechanical Engineering, Purdue University, West Lafayette, IN.

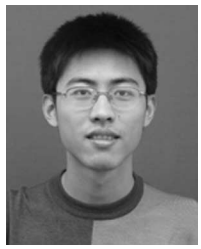

Zheng Chen received the B.Eng. degree in mechatronic engineering in 2007 from Zhejiang University, Hangzhou, China, where he is currently working toward the Ph.D. degree in mechatronic engineering.

Bin Yao (S'93–M'96) received the B.Eng. degree in applied mechanics from Beijing University of Aeronautics and Astronautics, Beijing, China, in 1987, the M.Eng. degree in electrical engineering from Nanyang Technological University, Singapore, in 1992, and the Ph.D. degree in mechanical engineering from the University of California, Berkeley, in February 1996.

Since 1996, he has been with the School of Mechanical Engineering, Purdue University, West Lafayette, IN, where he was promoted to the rank of Professor in 2007. He is also a Kuang-piu Professor at Zhejiang University, China. Since 2006, he has been an Associate Editor of the *ASME Journal of Dynamic Systems, Measurement, and Control*.

Prof. Yao was a recipient of the Faculty Early Career Development (CAREER) Award from the National Science Foundation (NSF) in 1998 and a Joint Research Fund for Outstanding Overseas Chinese Young Scholars from the National Natural Science Foundation of China (NSFC) in 2005. He was the recipient of the O. Hugo Schuck Best Paper (Theory) Award from the American Automatic Control Council in 2004 and the Outstanding Young Investigator Award of the American Society of Mechanical Engineers (ASME) Dynamic Systems and Control Division (DSCD) in 2007. He is a member of the ASME, and has chaired numerous sessions and served in a number of International Program Committees of various IEEE, ASME, and the International Federation of Automatic Control (IFAC) conferences. From 2000 to 2002, he was the Chair of the Adaptive and Optimal Control Panel, and from 2001 to 2003, the Chair of the Fluid Control Panel of the ASME Dynamic Systems and Control Division (DSCD). He is currently the Vice Chair of the ASME DSCD Mechatronics Technical Committee. He was a Technical Editor of the IEEE/ASME TRANSACTIONS ON MECHATRONICS from 2001 to 2005.

Qingfeng Wang received the M.Eng. and Ph.D. degrees in mechanical engineering from Zhejiang University, Hangzhou, China, in 1988 and 1994, respectively.

He was a faculty member at Zhejiang University, where he became a Professor in 1999, and from 2001 to 2005, was the Director of the State Key Laboratory of Fluid Power Transmission and Control. He is currently the Director of the Institute of Mechatronic Control Engineering. His current research interests include electrohydraulic control components and systems, hybrid power systems and energy-saving techniques for construction machinery, and system synthesis for mechatronic equipment.